Electronic Supplementary Material (ESI) for Soft Matter.

Coarse-grained molecular models of the surface of hair

Electronic Supplementary Information (ESI)

Erik Weiand[a,b,c,*], James P. Ewen[a,b,c,*], Peter H. Koenig[d], Yuri Roiter[d], Steven H. Page[d], Stefano Angioletti-Uberti[b,c,e], and Daniele Dini[a,b,c]

[a]Department of Mechanical Engineering, Imperial College London, South Kensington Campus, Sw7 2AZ London, U.K.
[b]Institute of Molecular Science and Engineering, Imperial College London, South Kensington Campus, Sw7 2AZ London, U.K.
[c]Thomas Young Centre for the Theory and Simulation of Materials, Imperial College London, South Kensington Campus, Sw7 2AZ London, U.K.
[d]Winton Hill Business Center, The Procter and Gamble Company, Cincinnati, 45224 Ohio, U.S.A.
[e]Department of Materials, Imperial College London, South Kensington Campus, Sw7 2AZ London, U.K.
[*]E-mails: erik.weiand19@imperial.ac.uk; j.ewen@imperial.ac.uk

A Force field parameters

Molar mass values in parenthesis are only valid for lipid terminal beads (C_1, C_2). Here, length units are given in Angstrom for consistency with LAMMPS *real* units. By convention, bond and angle constants are not multiplied by 1/2 in LAMMPS. Force field parameters are obtained from the original MARTINI model[1] for monolayer bead interactions and from the polarisable water model paper[2] for water-water, water-monolayer and charged bead interactions.

Bead Types		
Bead type	Charge q/e [-]	Molar mass M [kg/kmol]
C_1	-	72.0 (90.0)
C_2	-	72.0 (90.0)
C_5	-	72.0
P_5	-	72.0
Q_a	-1.0	72.0
Q_d	$+1.0$	72.0
N_a	-	72.0
W	-	24.0
WM	-0.46	24.0
WP	$+0.46$	24.0

Non-Bonded Interactions $E_{\mathrm{LJ}} = 4\varepsilon\left[\left(\frac{\sigma}{r}\right)^{12} - \left(\frac{\sigma}{r}\right)^{6}\right] + S_{\mathrm{LJ}}(r)$

Bead A	Bead B	Type[1,2]	ε [kcal/mol]	σ [Å]	Bead A	Bead B	Type[1,2]	ε [kcal/mol]	σ [Å]
C_1	C_1	IV	0.8365	4.7	C_5	P_5	V	0.7409	4.7
C_1	C_2	IV	0.8365	4.7	C_5	Q_a	IV	0.8365	4.7
C_1	C_5	V	0.7409	4.7	C_5	Q_d	IV	0.8365	4.7
C_1	P_5	VIII	0.4780	4.7	C_5	W	V	0.7034	4.7
C_1	Q_a	VII	0.5497	4.7	P_5	P_5	O	1.3384	4.7
C_1	Q_d	VII	0.5497	4.7	P_5	Q_a	O	1.3384	4.7
C_1	W	VIII	0.4538	4.7	P_5	Q_d	O	1.3384	4.7
C_2	C_2	IV	0.8365	4.7	P_5	W	O	1.2707	4.7
C_2	C_5	V	0.7409	4.7	Q_a	Q_a	IV	0.8365	4.7
C_2	P_5	VII	0.5497	4.7	Q_a	Q_d	III	0.9556	4.7
C_2	Q_a	VII	0.5497	4.7	Q_a	W	I	1.1942	4.7
C_2	Q_d	VII	0.5497	4.7	Q_d	Q_d	IV	0.8365	4.7
C_2	W	VII	0.5222	4.7	Q_d	W	I	1.1942	4.7
C_5	C_5	IV	0.8365	4.7	W	W	-	0.9554	4.7
WP	*	-	0	-	WM	*	-	0	-
C_1 (ghost)	*	-	0	-					

Bonds $E_{\mathrm{b}} = K_{\mathrm{b}}(r - r_0)$

Bead A	Bead B	K_b [kcal/mol/Å^2]	r_0 [Å]
C_*, P_*, Q_*	C_*, P_*, Q_*	1.4938	4.7
W	WM, WP	$K_b \to \infty$ (SHAKE)	1.2

Angles $E_\theta = K_\theta\left[\cos(\theta) - \cos(\theta_0)\right]^2$

Bead A	Bead B	Bead C	K_θ [kcal/mol]	θ_0 [°]
C_*, P_*, Q_*	C_*, P_*, Q_*	C_*, P_*, Q_*	2.9876	180
WM	W	WP	0.5019	0

B Lipid monolayer terminal bead comparison

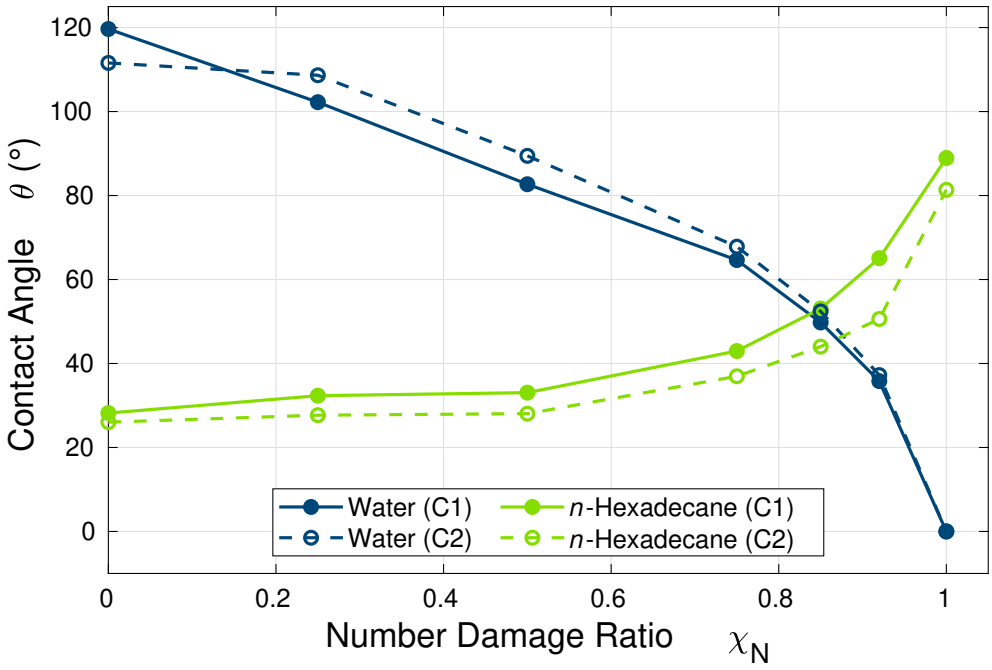

Figure 1 Water droplet contact angles on hair surfaces of various degrees of damage and C_1 and C_2 monolayer terminal beads with the original polarisable water model.[2] Contact angles are shown against the number damage ratio χ_N instead of the surface damage ratio χ_S to provide alignment of data points in the x position of the graph for better readability. Uncertainty bars are also omitted for improved readibility.

As expected, the surface became progressively less hydrophobic when transitioning from a C_1 (alkyl) to a C_2 (thioester) terminal bead. The trends found in this evaluation are comparable with the observations of water droplet wetting on an FCC surface.[3] The fully-functionalised system with the C_2 terminal bead was found to yield the best agreement with experimental data for water on virgin hair than the C_2 terminal bead.[4] For the slightly damaged surfaces, the systems with the C_2 terminal bead become more hydrophobic than the corresponding surfaces with a C_1 bead, despite the stronger LJ interactions between these beads and the water beads. This is because the stronger LJ interactions cause more agglomeration of the chains and thus less of the hydrophilic sulfonate surface is exposed. Moreover, C_2 bead leads to underestimation of the contact angle for non-polar fluids, such as *n*-hexadecane, on hair (see main text). Therefore, the C_1 terminal bead is selected for the final model version.

C CG water model comparison

Several coarse-grained water models were assessed by means of the surface tension at the water-vapor and water-hexadecane interface. Note that the surface tension at the hexadecane-vapour interface (24 mN/m) is the same for all of the *MARTINI*-based water models and is in good agreement with experiment (27 mN/m).[5] A slab configuration ($\mathscr{L}_x = 5.57$ nm, $\mathscr{L}_y = 5.57$ nm, $\mathscr{L}_z = 33.1$ nm) with a central water layer of initial thickness $d_z = 14.3$ nm was used for this purpose. This is sufficiently large in the x and y directions (11×11 σ^2) to prevent finite-size effects.[6] The results are shown below in Table 1 with reference values from the original papers where available. Long-range electrostatics were applied in the same manner as described in the Methodology section.

Table 1 Surface tension for water-vapor and water-hexadecane interfaces for different CG water models and reference experimental and simulation values

		Experiment	Orig. polarisable[2]	*refPol*[7]	BMW-MARTINI[8]	Ref. BMW-MARTINI[5]
$\gamma_{\mathrm{Wat-Vap}}$	[mN/m]	n/a	31	17	78	77
$\gamma_{\mathrm{Wat-Vap}}$(Ref)	[mN/m]	72[9]	31[2]	n/a	79[5]	79[5]
$\gamma_{\mathrm{Wat-Hex}}$	[mN/m]	n/a	40	34	96	65
$\gamma_{\mathrm{Wat-Hex}}$(Ref)	[mN/m]	54[10]	43[11]	n/a	93[5]	69[5]

Surface tension values reported in the reference publications differ slightly from our results in several instances. This is expected to be a result of differences in integration timesteps and the choice of cut-off length and/or long range solver used for the LJ potential and electrostatic interactions. Preliminary simulations showed a high sensitivity to the cut-off length in particular. Even at reasonably long r_c, both BMW-MARTINI models[5,8] suffered from freezing artefacts when departing from the bulk configuration towards a nanoscale droplet configuration. The *refPol* model provides improvements over the original polarisable model, such as better agreement of mass density and dielectric constant with respect to experimental values.[7] However, the water-vapor surface tension was not evaluated in the original publication and turns out to provide poor agreement compared to all the other models and the experimental reference. For that reason, we fall back to the original polarisable *MARTINI* model for water in our further analyses.[2]

It is to be stressed that the choice of integration timestep in LAMMPS is of utmost importance for producing valid results with the polarisable water models. For example, energy conservation in the NVE ensemble was not achieved for trial runs with the *BMW-MARTINI* model at timesteps of 10 and 20 fs. The timestep is therefore limited to 5 fs in LAMMPS, contrary to common simulation procedures for other codes such as Gromacs[12] as described in previous publications.[8]

The vast majority of available bottom-up CG water models have been designed to reproduce a set of specific validation parameters, but tend to lack generality which can ultimately limit their application to specific purposes deviating from design configurations. Droplet wetting has not been considered in the parametrisation of any of the water models above. Future CG water modeling efforts in the *MARTINI* framework should focus on an integrated approach, considering several optimization parameters including the surface tension and wetting behavior of nanoscale systems. The recently published MARTINI 3 force field[13] is a promising framework for integration of a suitable polarisable water model.

D Droplet size effects

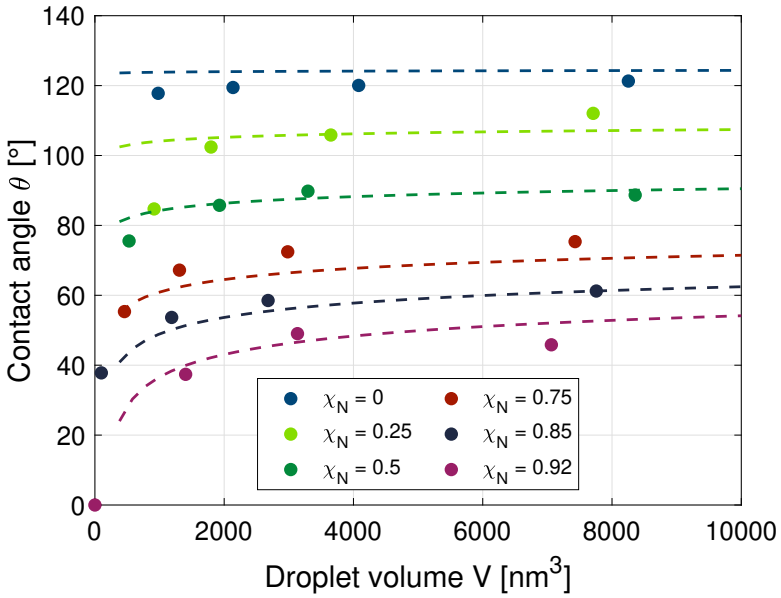

Figure 2 Water droplet contact angle as a function of actual droplet volume and damage ratio χ_N. Contact angle fits using a modified Cassie-Baxter relationship for *fuzzy interfaces*[14] ($m_i^{SL} = 0.5427$, $m_j^{SL} = 0.6725$) are shown by solid lines.

A modified Cassie-Baxter relationship for *fuzzy interfaces* is used to perform a volume-based fit to the contact angle simulation data:[14]

$$\cos\theta = \chi_S \cos\theta_{i,ref} \left(\frac{V}{V_{ref}}\right)^{m_i^{SL}-\frac{2}{3}} + (1-\chi_S)\theta_{j,ref} \left(\frac{V}{V_{ref}}\right)^{m_j^{SL}-\frac{2}{3}} \quad (1)$$

The fitting coefficients are m_i^{SL} and m_j^{SL} for a specified reference volume V_{ref} (here, volume of droplet with initial water unit count of $N = 18,121$) and reference contact angles (nominal fully-functionalized and fully damaged monolayer).

E Projected surface coverage

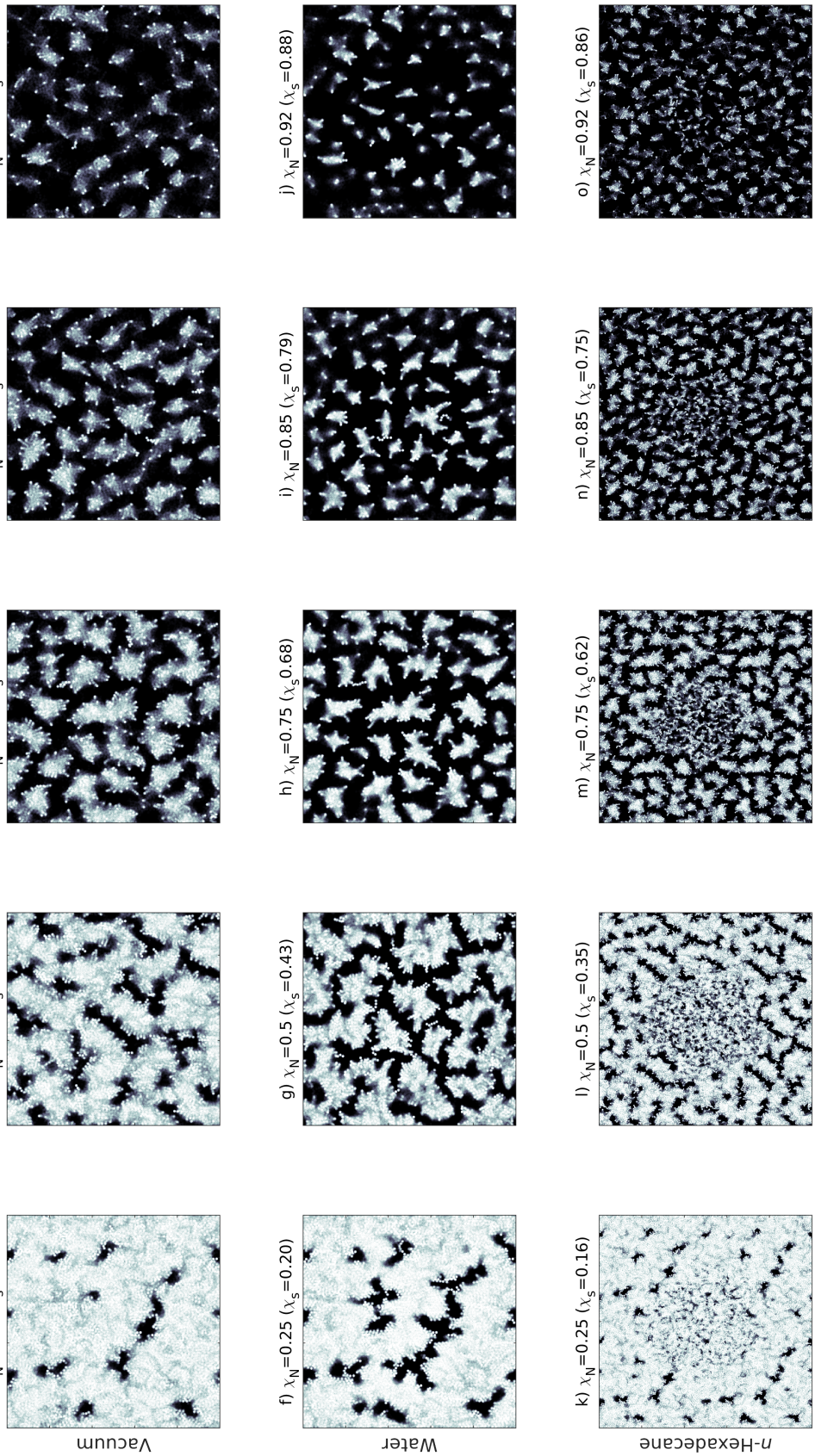

Figure 3 Projected lipid coverage on hair model surfaces in vacuum and with water and *n*-hexadecane as wetting fluids for different degrees of random damage χ_N. White regions correspond to coverage by at least one monolayer bead during all sampled timesteps while black regions indicate projected densities equal to zero. Projected surface coverage is given by χ_s. The time-averaged data have been sampled from 40 equidistant timesteps (10 for *n*-hexadecane) within the last 2 ns of each simulation. The shown coverage maps represent one periodic box of side lengths $\mathscr{L}_{x,\mathrm{water}} = 35.7$ ($\mathscr{L}_{x,\mathrm{hex}} = 71.5$) nm and $\mathscr{L}_{y,\mathrm{water}} = 30.9$ nm ($\mathscr{L}_{y,\mathrm{hex}} = 61.9$ nm).

F Contact angle fits

F.1 *n*-hexadecane

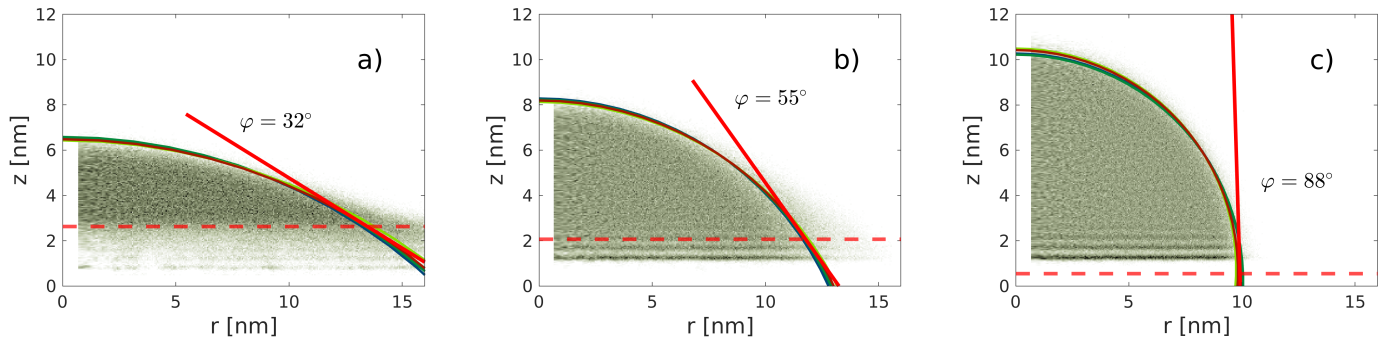

Figure 4 Circular surface fits of a *n*-hexadecane droplets on the a) fully-functionalised ($\chi_N = 0$) and partially damaged (b) $\chi_N = 0.85$ and fully damaged c) $\chi_N = 1$) monolayers from the CG-MD simulations. Four temporal bin fits for the droplet surface (solid circles) are shown. Averaged contact angles are indicated by bold red lines. The surface-normal position for the contact angle measurement is shown (dashed red line). Individual surface density fits in the radial direction are omitted for the sake of clarity.

F.2 Water (AA)

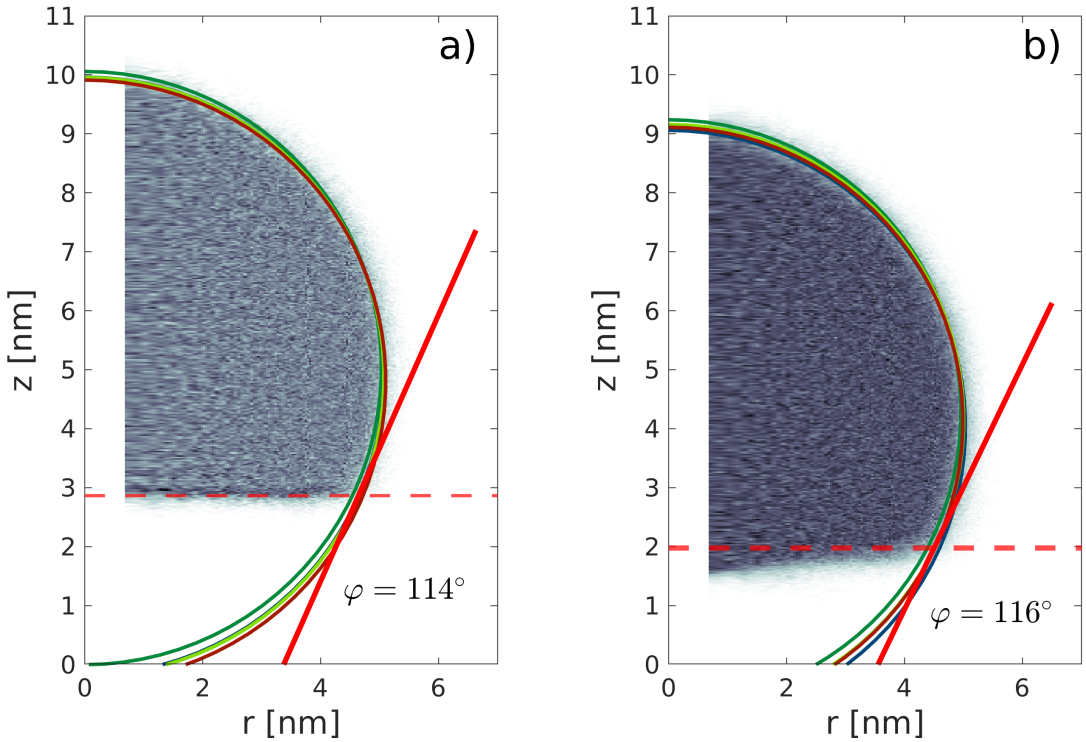

Figure 5 Circular surface fits of a water droplets on monolayers with a grafting distance of (a) $d_{graft} = 0.49$ nm and (b) $d_{graft} = 0.65$ nm from the AA-MD simulations. Four temporal bin fits for the droplet surface (solid circles) are shown. Averaged contact angles (solely from the shown four temporal bins) are indicated by bold red lines. The surface-normal position for the contact angle measurement is shown (dashed red line). Individual surface density fits in the radial direction are omitted for the sake of clarity.

G Wetting data

Table 2 Fully-functionalised monolayer structure and wetting data for all-atomistic (AA), coarse-grained (CG) MD cases and comparison to reference AA-MD data[15] for 18-MEA.

Property	Unit	d_{graft} [nm]	Cheong et al.[15] 18-MEA	AA-MD 18-MEA	CG-MD EA	CG-MD Cys-18-MEA
Monolayer thickness	[nm]	0.49	2.64	2.59	2.78	2.63
		0.65	2.01	2.03	2.19	1.53
Monolayer tilt angle	[°]	0.49	5.0	7.7	6.0	1.7
		0.65	50	45	33	45
Water penetration depth	[nm]	0.49	n/a	0.29	n/a	0.20
		0.65	n/a	1.29	n/a	0.85
Contact angle (water)	[°]	0.49	n/a	114	n/a	116
		0.65	n/a	116	n/a	120

Table 3 Contact angle data from CG-MD for the C_1 type terminal lipid beads at various degrees of random lipid damage - data for Fig. 6 in the main text.

	Water		*n*-hexadecane	
χ_N	χ_S	θ [°]	χ_S	θ [°]
0.00	0.00	120	0.00	28
0.25	0.20	102	0.16	32
0.50	0.43	83	0.35	33
0.75	0.68	65	0.62	43
0.85	0.79	50	0.75	53
0.92	0.88	36	0.86	65
1.00	1.00	0	1.00	89

H Wetting fluid penetration

H.1 Water

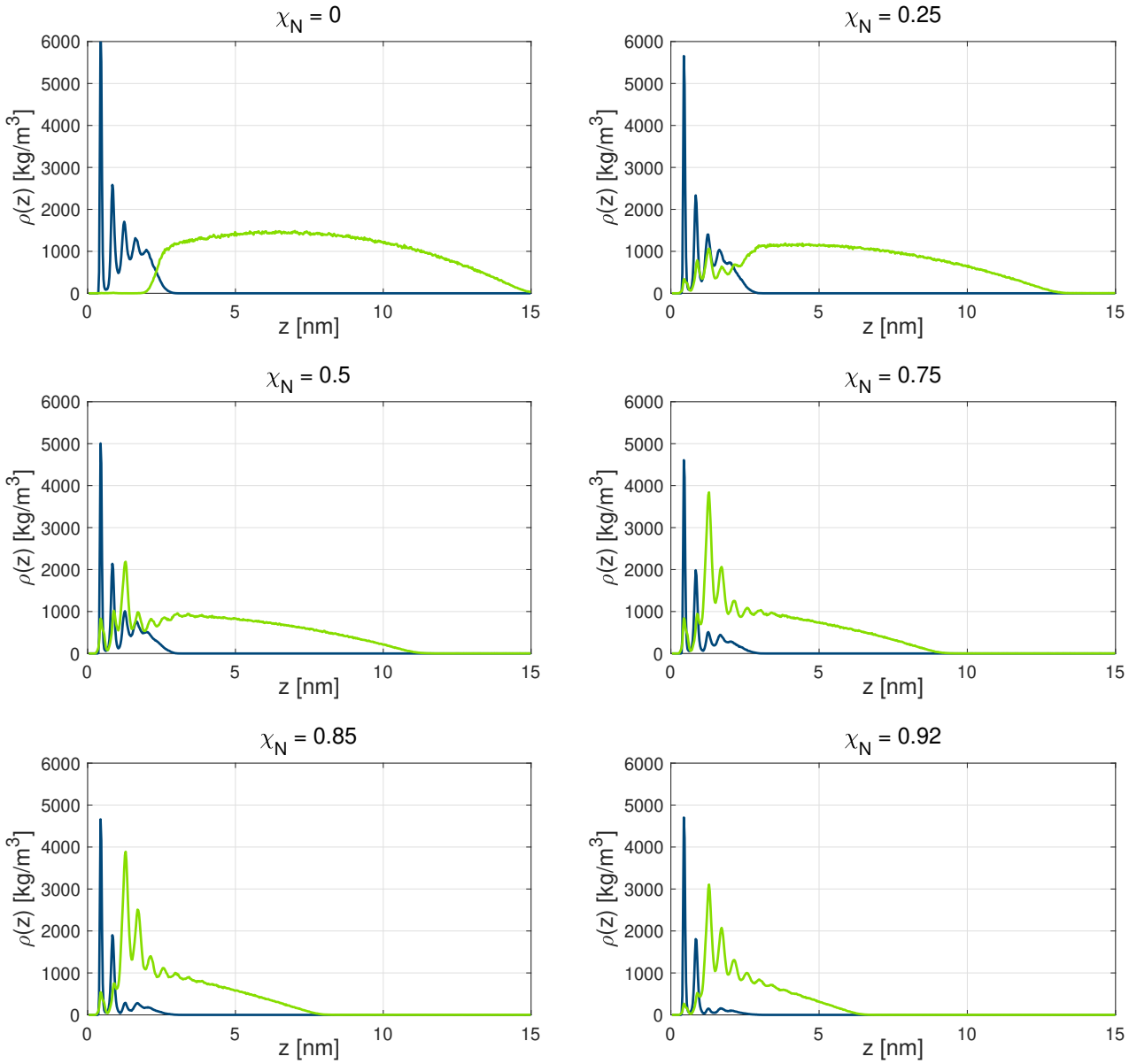

Figure 6 Coarse-grained monolayer and water density profiles along the surface-normal direction at different damage ratios χ_N. Water densities are re-scaled by the droplet area at the contact interface.

H.2 *n*-hexadecane

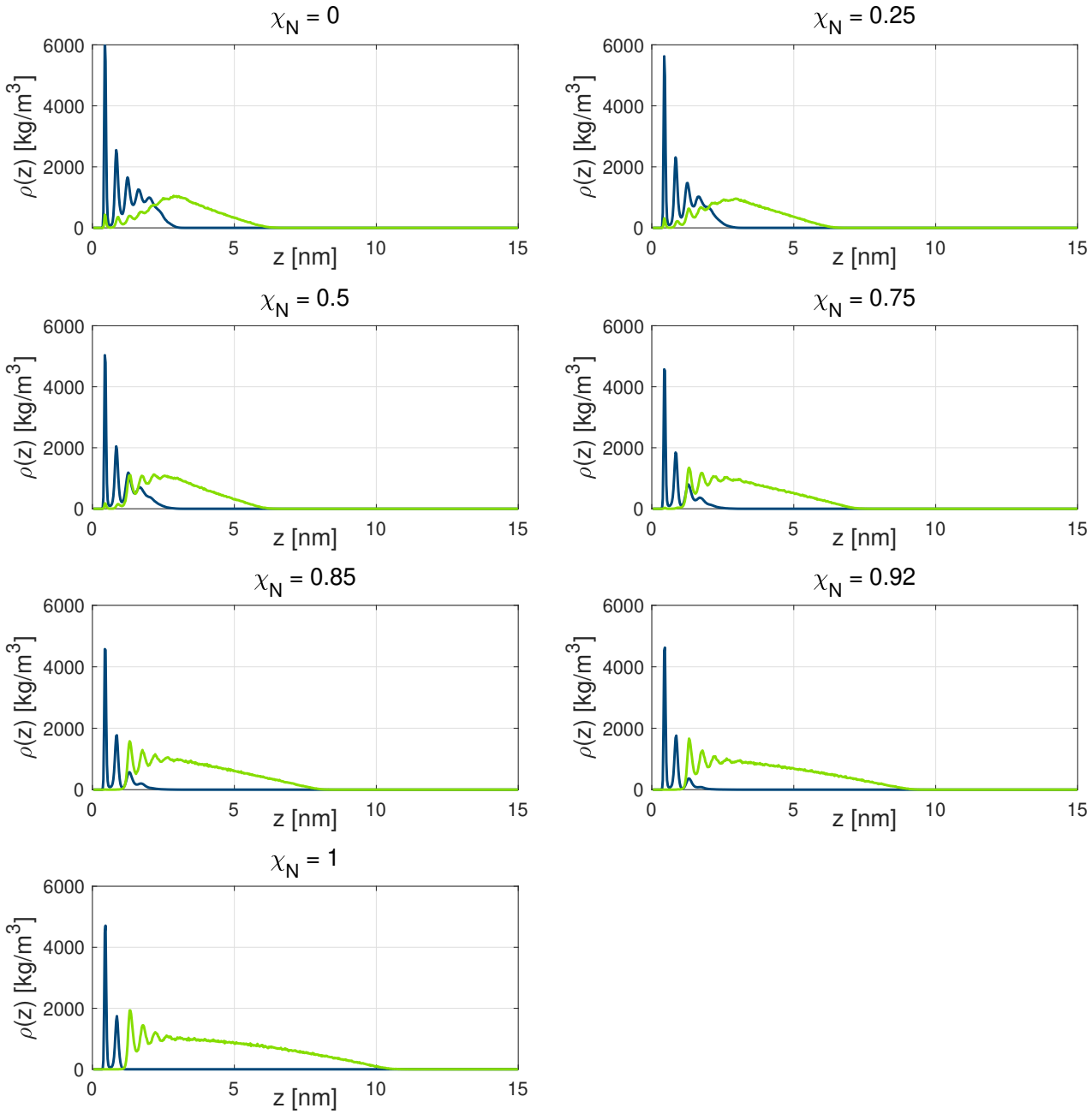

Figure 7 Coarse-grained monolayer and *n*-hexadecane density profiles along the surface-normal direction at different damage ratios χ_N. *n*-hexadecane densities are re-scaled by the droplet area at the contact interface.

H.3 CG-MD/AA-MD comparison

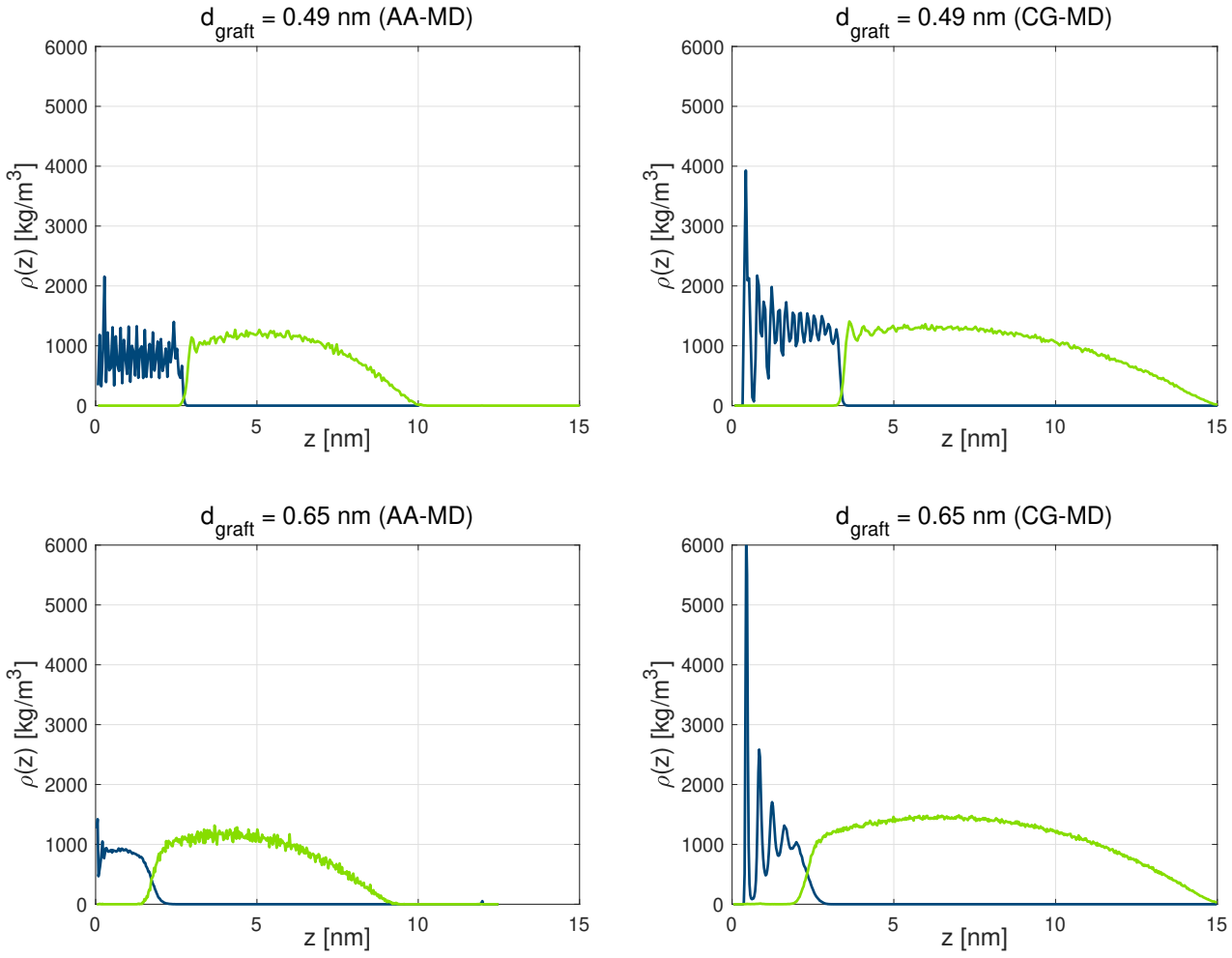

Figure 8 AA-MD and CG-MD water (green) and monolayer (blue) density profiles along the surface-normal direction for fully functionalised monolayers ($\chi_N = 0$) at grafting distances of $d_{\text{graft}} = 0.49$ nm (top) and $d_{\text{graft}} = 0.65$ nm (bottom). Water densities are re-scaled by the droplet area at the contact interface.

I Contact angle experimental comparison

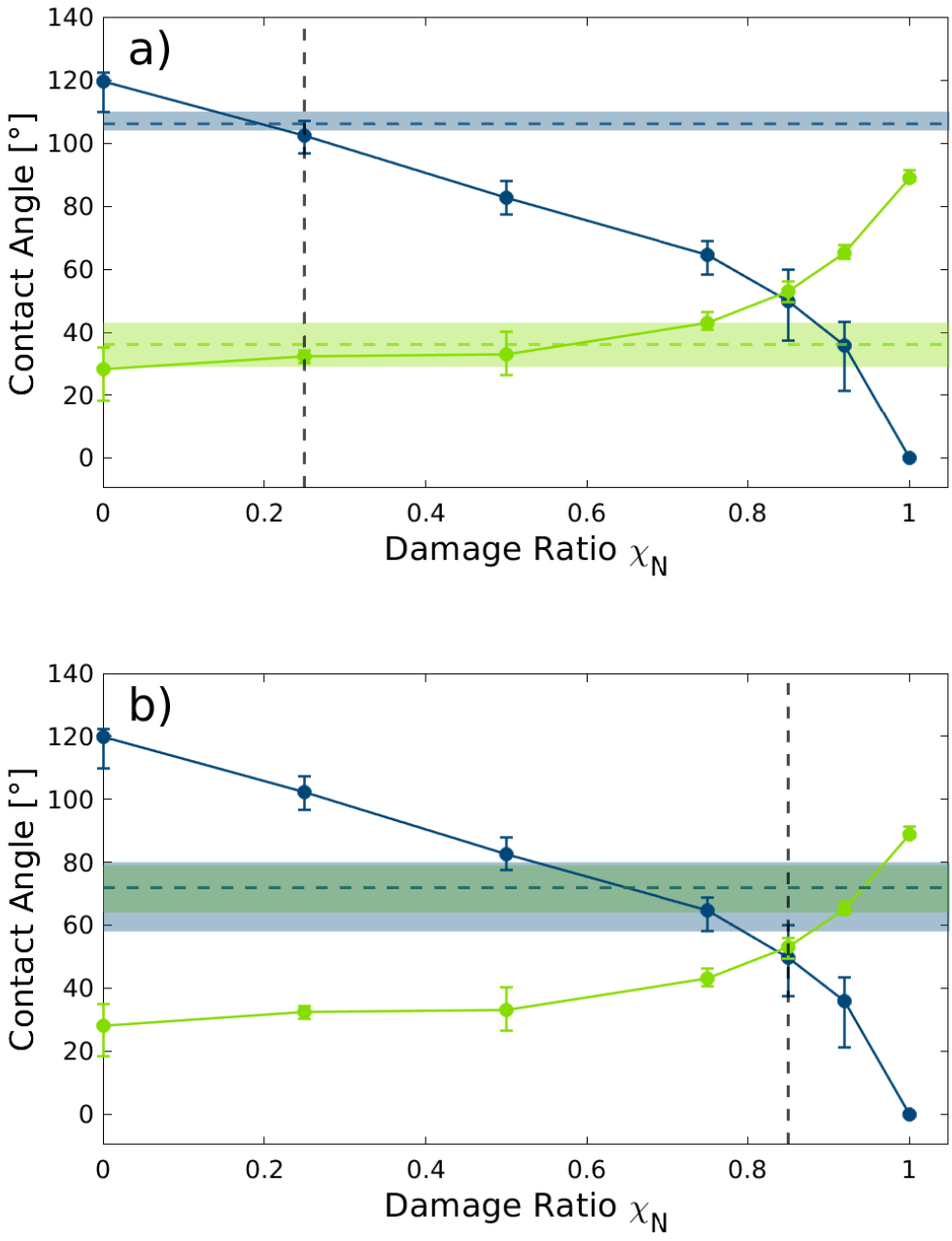

Figure 9 Water (blue) and *n*-hexadecane (green) droplet contact angles as a function of number damage ratio χ_N compared to dynamic contact angle measurements for a) virgin hair and b) medium bleached hair. For the simulations, the points are mean values and the vertical bars show the minimum and maximum values observed across the temporal binning of the different position and seed trials. Coloured solid lines are guides for the eye. Average experimental values are shown by horizontal dashed lines and the coloured regions represent the uncertainty limits. Good agreement between simulations and experiments is found when $\chi_N = 0.25$ for virgin hair and $\chi_N = 0.85$ for medium bleached hair, as indicated by vertical dashed lines in a) and b), respectively.

References

[1] S. J. Marrink, H. J. Risselada, S. Yefimov, D. P. Tieleman and A. H. De Vries, *J. Phys. Chem. B*, 2007, **111**, 7812–7824.

[2] S. O. Yesylevskyy, L. V. Schäfer, D. Sengupta and S. J. Marrink, *PLoS Comput. Biol.*, 2010, **6**, 1–17.

[3] A. Ramazani, T. Mandal and R. G. Larson, *Langmuir*, 2016, **32**, 13084–13094.

[4] E. S. Zur Wiesche, A. Körner, K. Schäfer and F.-J. Wortmann, *J. Cosmet. Sci.*, 2011, **62**, 237–249.

[5] V. Miguel, M. A. Perillo and M. A. Villarreal, *Biochim. Biophys. Acta*, 2016, **1858**, 2903–2910.

[6] F. Goujon, A. Dequidt, A. Ghoufi and P. Malfreyt, *J. Chem. Theory Comput.*, 2018, **14**, 2644–2651.

[7] J. Michalowsky, L. V. Schäfer, C. Holm and J. Smiatek, *J. Chem. Phys.*, 2017, **146**, 054501.

[8] Z. Wu, Q. Cui and A. Yethiraj, *J. Chem. Theory Comput.*, 2011, **7**, 3793–3802.

[9] N. B. Vargaftik, B. N. Volkov and L. D. Voljak, *J. Phys. Chem. Ref. Data*, 1983, **12**, 817–820.

[10] D. M. Mitrinović, A. M. Tikhonov, M. Li, Z. Huang and M. L. Schlossman, *Phys. Rev. Lett.*, 2000, **85**, 582–585.

[11] M. Ndao, J. Devémy, A. Ghoufi and P. Malfreyt, *J. Chem. Theory Comput.*, 2015, **11**, 3818–3828.

[12] H. J. Berendsen, D. van der Spoel and R. van Drunen, *Comput. Phys. Commun.*, 1995, **91**, 43–56.

[13] P. C. T. Souza, R. Alessandri, J. Barnoud, S. Thallmair, I. Faustino, F. Grünewald, I. Patmanidis, H. Abdizadeh, B. M. H. Bruininks, T. A. Wassenaar, P. C. Kroon, J. Melcr, V. Nieto, V. Corradi, H. M. Khan, J. Domański, M. Javanainen, H. Martinez-Seara, N. Reuter, R. B. Best, I. Vattulainen, L. Monticelli, X. Periole, D. P. Tieleman, A. H. de Vries and S. J. Marrink, *Nat. Methods*, 2021, **18**, 382–388.

[14] P. Letellier, A. Mayaffre and M. Turmine, *J. Colloid Interface Sci.*, 2007, **314**, 604–614.

[15] D. W. Cheong, F. C. Lim and L. Zhang, *Langmuir*, 2012, **28**, 13008–13017.